Characterizing the 1,4-Dihydropyridines Binding Interactions in the L-Type Ca^{2+} Channel: Model Construction and Docking Calculations

Sandro Cosconati,* Luciana Marinelli, Antonio Lavecchia, and Ettore Novellino*

Dipartimento di Chimica Farmaceutica e Tossicologica, Università di Napoli "Federico II", Via D. Montesano 49, 80131 Napoli, Italy

Received October 23, 2006

L-type Ca^{2+} channels (LCC) are membrane heteromultimeric proteins that allow the selective entrance of Ca^{2+} ions into excitable cells upon membrane depolarization. Despite the large amount of compounds (1,4-dihydropyridines, phenylalkylamines, and benzothiazepines) that impede the passage of Ca^{2+} ions through the channel, it is still not clear how these molecules bind to LCC at an atomic level. In this study, a 3D model of the central pore of LCC was constructed using the X-ray structure of the KcsA K^+ channel as template. The resulting LCC model was then used to dock nine different DHPs to shed light on their binding mode. The accordance between the developed model and several experimental data gives us the confidence to propose our model as a valuable platform for future studies aimed at the identification of new potent and LCC-selective ligands.

Introduction

Ca^{2+} channels are transmembrane proteins that, upon membrane depolarization, allow the selective passage of Ca^{2+} ions into excitable cells. By controlling the entry of Ca^{2+} into cells, these proteins have a critical role in a broad range of cellular processes, such as neurotransmitter release, second messenger cascades, cardiac excitation and contraction, and gene regulation supporting learning and memory.[1] The Ca^{2+} channel family contains at least ten members that are distinguished by their structure, subunit composition, location, biophysical properties, and pharmacology. According to their electrophysiological and pharmacological properties, Ca^{2+} channels are distinguished in N-, L-, T-, P/Q-, and R-type channels.[2] Among these, the L-Type Ca^{2+} channel (LCC) has been extensively characterized through biochemical studies, revealing that LCCs are heteromultimeric proteins consisting of an α_1 subunit, which, forming the central pore, expresses the major biophysical, functional and pharmacological properties of the channel. The α_1 subunit is associated with a number of auxiliary subunits, such as α_2, β, γ, and δ, that control channel expression, membrane incorporation, drug binding, and the gating characteristics of the central unit.[3] Analogously to the structurally homologous K^+ and Na^+ channels,[4] the α_1 subunit of LCC is made by four domains (repeat I−IV) each consisting of six transmembrane α-helical segments (S1−S6). The central pore of LCC is formed by the S6 segment of each subunit and by the extracellular region between S5 and S6 segments (P-loop) that deepens into the pore, forming the extracellular mouth of the channel. Four conserved Glu residues, in the four P-loops, form the so-called EEEE locus which acts as a selectivity filter for the passage of Ca^{2+} and other divalent ions.[5]

To date, just three different chemical categories of LCC-targeting drugs exist: 1,4-dihydropyridines (DHPs such as nifedipine), phenylalkylamines (PAAs such as verapamil), and benzothiazepines (BTZs such as diltiazem).[6] They are extensively used in the treatment of cardiovascular disorders, including hypertension, arrhythmias, angina, and central and peripheral vascular disorders.[7] While verapamil and diltiazem are the only therapeutically available members of their respective families, DHPs are well represented by several second and third-generation agents. The binding domains of these drugs were extensively probed by radiolabeled ligands in particulate and purified Ca^{2+} channel preparations.[8] These studies clearly revealed that the different chemical classes of Ca^{2+} channel antagonists do not interact with the same binding site on α_1 subunit. Instead, they noncompetitively affect each other's binding and also interfere with Ca^{2+} binding to the channel. Several studies conducted by Hockerman and co-workers indicated that PAAs reach their binding site from the cytoplasm and are considered to be pore-blocking drugs that block LCC directly by occluding the transmembrane pore through which Ca^{2+} ions move.[8] In contrast, DHPs bind to a single site at which agonists increase Ca^{2+} channel activity and antagonists reduce it.[8] Therefore, DHP antagonists are believed to block the pore indirectly by stabilizing a channel closed state with a single Ca^{2+} ion bound in a blocking position in the pore. In fact, site-directed mutagenesis experiments confirmed that the binding of Ca^{2+} to the selectivity filter stabilizes the DHP receptor in its high affinity closed state.[9] Despite the large body of evidence regarding the specific residues involved in the binding of these drugs together with the extensive structure−activity relationships (SARs) data on the different compounds, it is still not absolutely clear how these molecules actually bind to LCC. Because the three-dimensional (3D) structure of LCC is not available, two theoretical models of this channel have been developed so far. In pioneering studies by Lipkind and Fozzard[10] and Zhorov and co-workers,[11] the binding pose of a few DHPs in LCC was also disclosed. While a manual docking procedure was adopted by Lipkind and Fozzard, Zhorov and co-workers docked nifedipine using a Monte Carlo minimization method. Unfortunately, the small number of docked ligands impedes to verify the consistency of the predicted ligand−protein complexes with the wide amount of experimental data.

Therefore, in the present study, we attempted to get major insights on the specific interactions between DHP antagonists and LCC by constructing a new model of the central pore region of the human LCC α_{1c} subunit ($Ca_v1.2$). In regard to the construction of the pore region of LCC, the X-ray crystal structure of the bacterial K^+ channel (KcsA) was used.[12] KcsA is made up of four subunits each consisting of only two

* To whom correspondence should be addressed. Phone and Fax: +39-81-678644. E-mail: scoscona@unina.it, novellin@unina.it.

10.1021/jm061245a CCC: $37.00 © 2007 American Chemical Society
Published on Web 03/03/2007

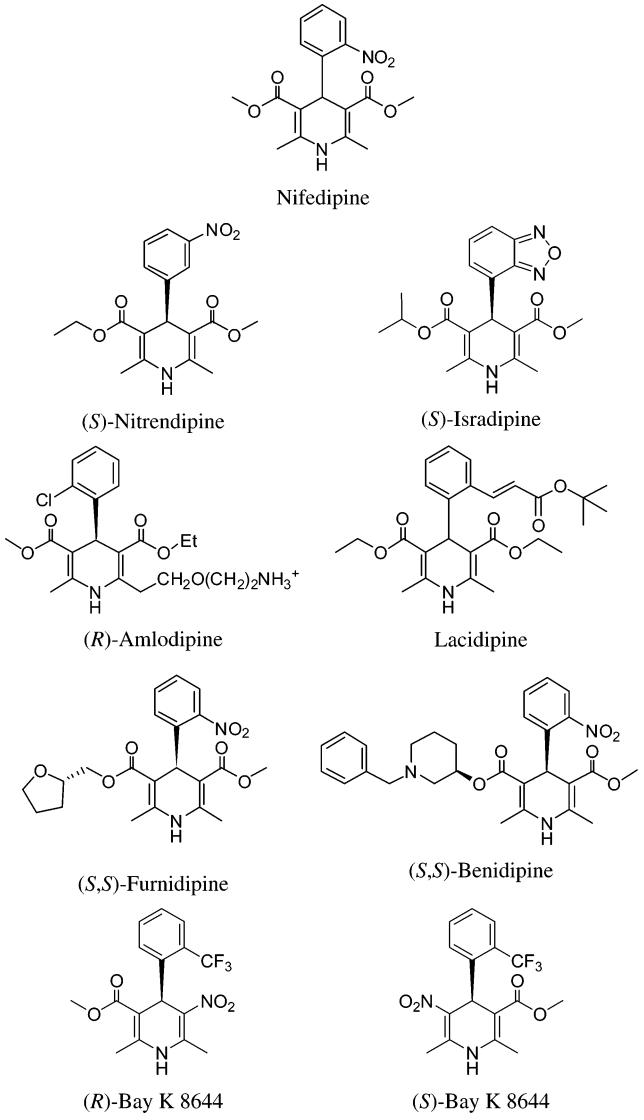

Figure 1. Structures of the investigated ligands.

transmembrane α-helical segments (M1 and M2) connected by an extracellular loop. Unlike LCC, KcsA is a homotetrameric rather than an eteromeric protein. Nowadays, it is accepted that KcsA architecture might describe also the pore of K^+, Na^+, Ca^{2+}, and other ion channels and, thus, it seems that KcsA is an evolutionary predecessor of the six-transmembrane segment ion channels.[13] More recently, Jiang et al. have determined the 3D structure of the open Ca^{2+}-activated K^+ channel MthK.[14] This structure is almost identical to KcsA apart from a hinge region in the M2 segment made of some glycine residues critical in the activation of this channel. Considering that voltage-opened Ca^{2+} channels have larger residues in the corresponding positions and the above cited turning point would not be feasible, the construction of the transmembrane portion of LCC using the MthK as a template does not seem viable.

The developed LCC model was then used to dock several DHPs (Figure 1). The ligand−channel complexes were predicted using the widely used automated docking software, AutoDock.[15,16] Hereafter, to distinguish between the two sides of the DHP ring, as suggested by Goldmann et al., the preferred conformation of the DHP ring will be regarded as a flattened boat with C4 as the bow, the axial aryl ring as the bowsprit, and the N1 atom as the stern (Figure 2a). Accordingly, the two sides of the DHP ring will be referred as the port side (left) and the starboard side (right; Figure 2b).[17]

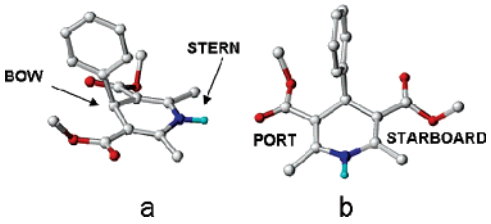

Figure 2. General structure of DHP drugs, with the adopted nomenclature highlighted.

```
KcsA
M1                  AGAATVLLVIVLLAGSYLA 47
CAC1C_HUMAN
IS5                 IALLVLFVIIYAIIGLELF 290
IIS5                LLLLFLFIIIFSLLGMQLF 673
IIIS5               VIVTTLLQFMFACIGVQLF 1071
IVS5                ALLIVMLFFIYAVIGMQVF 1430

KcsA
P                   ITYPRALWWSVETATTVGYGD 80
CAC1C_HUMAN
IP                  DNFAFAMLTVFQCITMEGWTD 367
IIP                 DNFPQSLLTVFQILTGEDWNS 710
IIIP                DNVLAAMMALFTVSTFEGWPE 1138
IVP                 QTFPQAVLLLFRCATGEAWQE 1468


KcsA
M2        I         WGRCVAVVVMVAGITSFGLVTAALAT 112
CAC1C_HUMAN
IS6                 WPWIYFVTLIIIGSFFVLNLVLGVLS 405
IIS6                LVCIYFIILFICGNYILLNVFLAIAV 753
IIIS6 (MODEL A)     VEISIFFIIYIIIIAFFMMNIFVGFV 1185
IIIS6 (MODEL B)     EISIFFIIYIIIIAFFMMNIFVGFVI 1186
IVS6                FAVFYFISFYMLCAFLIINLFVAVIM 1524
```

Figure 3. Pairwise alignment of CAC1C_HUMAN and KcsA sequences. The conserved key residues used to align the sequences are shown in red boxes. Residues reported to affect DHP antagonist binding and underscored and highlighted in bold.

Docking experiments were conducted on a selection of seven antagonist DHPs featuring structural diversity and for which enough experimental data were present in literature (Figure 1). For those compound with unsymmetrical ester substitution, a stereogenic center was present, and only the most active isomer was taken into account. Following this criteria, nifedipine,[18] (*S*)-nitrendipine,[19] lacidipine,[20] (*S*)-isradipine,[21] (*R*)-amlodipine,[22] (*S*,*S*)-furnidipine[23] and (*S*,*S*)-benidipine[24] were selected for this inspection. Some DHPs display a peculiar pharmacological behavior when the absolute configuration of their chiral center at position 4 is changed from the (*R*)-configuration to the (*S*)-configuration. In fact, while the first one has LCC-antagonist properties, the latter is an activator of this channel. This is the case of Bay K 8644, and for these reasons, both isomers of this ligand were also docked.

Altogether, our study provides for the first time a detailed description of the main interactions between LCC and DHP ligands. The consistency of the predicted binding poses with SARs and mutagenesis data supports the feasibility of our results.

Computational Methods

Molecular modeling and graphics manipulations were performed using the Sybyl 7.2[25] and InsightII[26] software packages, running on a Silicon Graphics Tezro workstation equipped with four 700 MHz R16000 processors. Energy minimizations and molecular dynamics (MD) simulations were realized by employing the module

Table 1. Results of Mutagenesis Experiments on LCC Using Different DHPs

segment	WT residue in rabbit LCC	WT residue in human LCC	mutant residue	mutant IC_{50}/WT IC_{50}	ref
IVS6	Tyr1463	Tyr1508	Ala	6.1	39
	Met1464	Met1509	Ala	1.6	39
	Ile1471	Ile1516	Ala	2.7	39
	Tyr1152	Tyr1169	Ala	25	40
			Phe	12.4	40
IIIS6	Ile1153	Ile1170	Ala	6.2	40
	Ile1156	Ile1173	Ala	17	40
	Met1160	Met1177	Ala	3.5	40
	Met1161	Met1178	Ala	9.6	40
	Thr1056	Thr1066	Tyr	>1000	37, 42
IIIS5			Ala	1	37,8
	Gln1060	Gln1070	Met	29.4	37, 8
IIIP	Phe1112	Phe1128	Ala	5.1	9, 48
	Ser1115	Ser1131	Ala	39.4	9, 48

Discover3[26] within InsightII, selecting the consistence-valence force field (CVFF).[27]

Construction of the Human LCC Model. The structural model of the human LCC was built using the recently reported 3.20 Å crystal structure of KcsA[12] (PDB entry code 1BL8) as a structural template. The sequence of the human LCC pore region α_{1c} subunit ($Ca_v1.2$, CAC1C_HUMAN) was retrieved from the SWISS−PROT database[28] and aligned as described in the Results and Discussion section (Figure 3). The construction of the transmembrane region of the two alternative models (Models A and B) was achieved with the employment of the Homology module within InsightII, which was also used to check the consistence of bond distances, bond angles, and torsion angles with protein standard values. After construction of the transmembrane region of both Model A and Model B, the whole structures were energetically minimized using the Discover3[26] module of the InsightII suite of programs with 5000 steps of the steepest descent minimization reaching a convergence of 10.0 kcal mol^{-1} $Å^{-1}$, followed by 3000 steps of conjugate gradient minimization reaching a final convergence of 0.01 kcal mol^{-1} $Å^{-1}$ to eliminate any residual geometrical strain, keeping the backbone atoms fixed. The same procedure was also followed for the construction of the P-loop region of LCC (for sequence alignment, see Figure 3).

After construction of both P-loop and transmembrane regions for Models A and B, the extracellular and transmembrane portion were assembled using the a protein−protein docking program. ZDOCK[29] software was used for rigid-body docking of the P-loop on the transmembrane region of LCC. This docking method is based on the FFT correlation approach[30] that systematically evaluates a simple grid-based scoring function over billions of relative orientations of the two proteins. ZDOCK scoring function includes a combination of shape complementarity, Coulombic electrostatics, and desolvation free energy based on the Zhang et al.[31] atomic contact potential. As default, ZDOCK retains 2000 structures. FFT-based tools are used to rapidly generate a large number of protein−protein conformations with good shape complementarity and with relatively favorable electrostatics and desolvation values. The top 20 000 structures were retained and ranked by the automated Cluspro web server (http://nrc.bu.edu/cluster).[32] The 30 different models achieved from the docking run were then analyzed according to the arrangement of the P-loop region on the transmembrane bundle. The best solutions for Models A and B were then used as the initial structure for the subsequent MD simulation. The selectivity-filter area of LCC contains eight negatively charged residues that are not counterbalanced by any positively charged one. Because Ca^{2+} ions should be the ones that are more present in this channel, four Ca^{2+} ions were added to the P-loop region to interact with the above cited acidic residues. The MD calculation was then begun with an initial and equilibration stage (500 ps), followed by a production run (1000 ps). In the equilibration stage, energy minimization of the protein side chains were achieved employing 3000 steps of steepest descent. Subsequently, the system was heated gradually starting from 10 to 310 K in 1 ps steps. The system was then equilibrated with a temperature bath coupling (310 K) applying a tethering force on the backbone starting from 100 kcal/$Å^{-2}$ and decreasing to 20 kcal/$Å^{-2}$. A cutoff of 18 Å was used for nonbonded interactions. Coordinates and energies of the production run were saved every 10 ps, yielding 100 structures. The average structure was calculated over the 100 structures of the production run and was energy-minimized using 3000 steps of a steepest descent minimization keeping the backbone atoms constrained. The stereochemical quality of the final structure was analyzed using the program PROCHECK.[33]

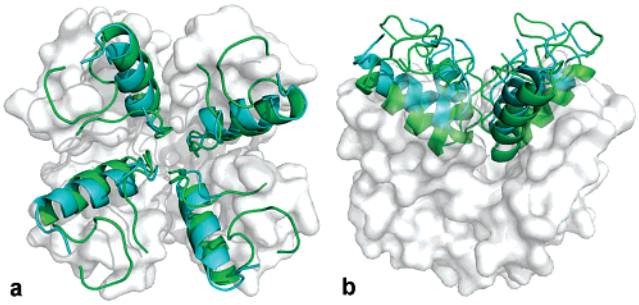

Figure 4. LCC model compared with the KcsA crystal structure. LCC transmembrane bundle is represented as a white transparent surface. The LCC P-loop is represented as a cyan ribbon, while the KcsA loop region is represented as a green ribbon.

Docking Simulations. Docking of nifedipine, (*S*)-nitrendipine, (*S*)-isradipine, (*R*)-amlodipine, lacidipine, (*S*,*S*)-furnidipine, and (*S*,*S*)-benidipine was performed with version 3.05 of the AutoDock software package.[15] It combines a rapid energy evaluation through precalculated grids of affinity potentials with a variety of search algorithms to find suitable binding positions for a ligand on a given protein. While the protein is required to be rigid, the program allows torsional flexibility in the ligand. Docking to LCC was carried out using the empirical free energy function and the Lamarckian genetic algorithm, applying a standard protocol, with an initial population of 50 randomly placed individuals, a maximum number of 1.5×10^6 energy evaluations, a mutation rate of 0.02, a crossover rate of 0.80, and an elitism value of 1. Proportional selection was used, where the average of the worst energy was calculated over a window of the previous 10 generations. For the local search, the so-called pseudo-Solis and Wets algorithm was applied using a maximum of 300 iterations per local search. The probability of performing the local search on an individual in the population was 0.06, and the maximum number of consecutive successes or failures before doubling or halving the local search step size was 4. A total of 50 independent docking runs were carried out for each ligand. Results differing by less than 1.5 Å in positional rmsd were clustered together and represented by the result with the most favorable free energy of binding.

Ligand Setup. The core structures of all ligands were retrieved from the Cambridge Structural Database (CSD)[34] and modified using standard bond lengths and bond angles of the Sybyl fragment library. Geometry optimizations were realized with the Sybyl/Maximin2 minimizer by applying the BFGS (Broyden, Fletcher, Goldfarb, and Shannon) algorithm[35] and setting a rmsd gradient of the forces acting on each atom of 0.05 kcal/mol Å as the convergence criterion. Atomic charges were assigned using the Gasteiger−Marsili formalism,[36] which is the type of atomic charges used in calibrating the AutoDock empirical free energy function. Finally, all compounds were set up for docking with the help of AutoTors, the main purpose of which is to define the torsional degrees of freedom to be considered during the docking process. The number of flexible torsions defined for each ligand is two for nifedipine, three for (*S*)-nitrendipine, (*S*)-isradipine, and (*R*)- and (*S*)-Bay K 8644, seven for (*R*)-amlodipine, six for lacidipine, four for (*S*,*S*)-furnidipine, and five for (*S*,*S*)-benidipine.

Protein Setup. Both Model A and Model B of LCC were set up for docking as follows: only polar hydrogens were added using

Table 2. Result of 50 Independent Docking Runs for Each DHP[a]

LCC model	ligand	N_{tot}	f_{occ}	ΔG_{bind}	surrounding residues
A	nifedipine	7	23	−8.33	**Gln1060** (IIIS5), Phe1061 (IIIS5), Ala1064 (IIIS5), Phe1128 (IIIP), **Ser1131** (IIIP), Thr1132 (IIIP), **Phe1133** (IIIP), **Tyr1169** (IIIS6), **Ile1170** (IIIS6), Ile1172 (IIIS6), **Ile1173** (IIIS6), Ala1174 (IIIS6), Phe1176 (IIIS6), **Met1177** (IIIS6), **Met1178** (IIIS6), Ile1180 (IIIS6), Ile1505 (IVS6), **Tyr1508** (IVS6), **Met1509** (IVS6), Ala1512 (IVS6), Phe1513 (IVS6)
	(*S*)-nitrendipine	10	19	−7.94	
	(*S*)-isradipine	9	17	−7.65	
	(*R*)-amlodipine	20	14	−8.07	
	lacidipine	20	18	−8.12	
	(*S*,*S*)-furnidipine	10	18	−9.49	
	(*S*,*S*)-benidipine	23	13	−9.93	
	(*R*)-benidipine	9	15	−8.74	
	(*S*)-Bay K 8644	13	10	−7.43	
B	nifedipine	5	18	−7.21	**Gln1060** (IIIS5), Phe1061 (IIIS5), Phe1063 (IIIS5), Ala1064 (IIIS5), Cys1065 (IIIS5), Leu1127 (IIIP), Phe1128 (IIIP), Thr1129 (IIIP), Val1130 (IIIP), **Ser1131** (IIIP), Thr1132 (IIIP), **Phe1133** (IIIP), Ile1168 (IIIS6), **Tyr1169** (IIIS6), **Ile1170** (IIIS6), Ile1171 (IIIS6), Ile1172 (IIIS6), **Ile1173** (IIIS6), Ala1174 (IIIS6), **Phe1175** (IIIS6), Phe1176 (IIIS6), **Met1177** (IIIS6), Phe1504 (IVS6), Ile1505 (IVS6), Ser1506 (IVS6), Phe1507 (IVS6), **Tyr1508** (IVS6), **Met1509** (IVS6), Leu1510 (IVS6), Ala1512 (IVS6), Phe1513 (IVS6), **Thr1056** (IVS6), Thr1057 (IVS6)
	(*S*)-nitrendipine	8	15	−7.18	
	(*S*)-isradipine	6	27	−7.44	
	(*R*)-amlodipine	24	10	−7.05	
	lacidipine	14	13	−7.00	
	(*S*,*S*)-furnidipine	11	21	8.22	
	(*S*,*S*)-benidipine	22	14	−8.77	

[a] N_{tot} is the total number of clusters; the number of results in the top cluster is given by the frequency of occurrence, f_{occ}; ΔG_{bind} is the estimated free energy of binding for the top cluster results and is given in kcal/mol. The last column shows the contacting residues for the binding mode of the best cluster solution calculated (*S*,*S*)-benidipine. Only residues located within 5 Å from any atom of the docked ligand are reported. Residues reported to influence DHP binding are highlighted in bold.

the biopolymers module of the Sybyl program (Arg, Lys, Glu, and Asp residues were considered ionized, while all His were considered neutral by default), and Kollman united-atom partial charges were assigned. Solvation parameters were added to the final protein file using the addsol utility of AutoDock. The grid maps representing the proteins in the actual docking process were calculated with AutoGrid. The grids (one for each atom type in the ligand, plus one for electrostatic interactions) were chosen to be sufficiently large to include not only the active site but also significant portions of the surrounding surface. The dimensions of the grids were thus 60 Å × 60 Å × 60 Å, with a spacing of 0.375 Å between the grid points.

Energy Refinement of DHPs/LCC Complexes. Refinement of the predicted DHP/LCC complexes was achieved through energy minimizations using the Discover3 module of InsightII. These geometric optimizations included 5000 steps of a steepest descent minimization, reaching a convergence of 10.0 kcal mol^{-1} $Å^{-1}$, followed by 3000 steps of conjugate gradient minimization, reaching a final convergence of 0.01 kcal mol^{-1} $Å^{-1}$, keeping the backbone atoms fixed and LCC side-chains and the ligand free to move.

Results and Discussion

Construction of LCC Transmembrane Bundle. When modeling a protein on a template structure, sequence alignment is the most important stage. In regard to the construction of a model of the central pore of LCC, this task becomes really challenging due to the low sequence identity between the KcsA and the LCC. In consonance with what was suggested by other authors,[10,11] we aligned the LCC sequence of the central pore with that corresponding to the KcsA tacking into account all possible experimental data present in literature. Photoaffinity labeling, construction of chimeric channels, and mutagenesis experiments all demonstrated that the IIIS6, IVS6, and IIIS5 transmembrane segments interact with the known LCC antagonists.[37] Most precisely, from mutagenesis studies (see Table 1 for a complete list of mutations), it clearly emerges that, in IVS6 segment, Tyr1508, Met1509, and Ile1516 are critical for the DHPs binding.[39,40] As concerns the IIIS6 segment, several residues influence the binding of DHPs, and these are Tyr1169, Ile1170, Ile1173, Met1177, and Met1178,[41]while in the case of the IIIS5 segment, Thr1066 and Gln1070 result to affect the DHP binding.[38,43] However, mutational data, although a precious source of information, should be treated with caution. In fact, one mutant can structurally change the binding site, either in shape or in flexibility, or it can hinder movement distal to the binding site, thereby altering the ligand binding or the signaling mechanism without necessarily changing a direct interaction with a ligand, such as a salt bridge, hydrogen bond, or hydrophobic stabilization. Nevertheless, Tyr1508 and Tyr1169 are thought to directly participate in the DHP binding, and certainly all this data indicate that DHPs interact with the LCC by binding between the IIIS6 and the IVS6 helices.[9]

As suggested by Lipkind and Fozzard, two different sequence alignments of the LCC transmembrane segments with KcsA can be hypothesized.[10] In regard to the IVS6 segment, it has been proposed to align the M2 Trp87 residue of KcsA with the hydrophobic residue Phe1499. This alignment would allow on one hand Tyr1508 to face the pore in accordance with mutagenesis data that demonstrate its important role in binding with the DHPs, and on the other hand, it locates Ile1173 to form the bottom of the putative binding site.[10,11]

In regard to the alignment of the IIIS6 segment to M2 of KcsA, two possibilities were given. In a first alignment, Glu1161 is aligned with Trp87 of KcsA, thus allowing Tyr1169, Ile1170, Ile1173, Met1177, and Met1178 to be located at the IIIS6−IVS6 interface. Alternatively, Val1160 can be aligned with Trp87, and this option would place Tyr1169 and Tyr1508 at the same level. It is worth noting that with the latter alignment, Ile1170 and Met178, which mutagenesis data indicate as important residues for DHP binding, are placed outside the pore. Indeed, the preference for one of the two proposed alignments of the segment IIIS6 of LCC with M2 of KcsA cannot be

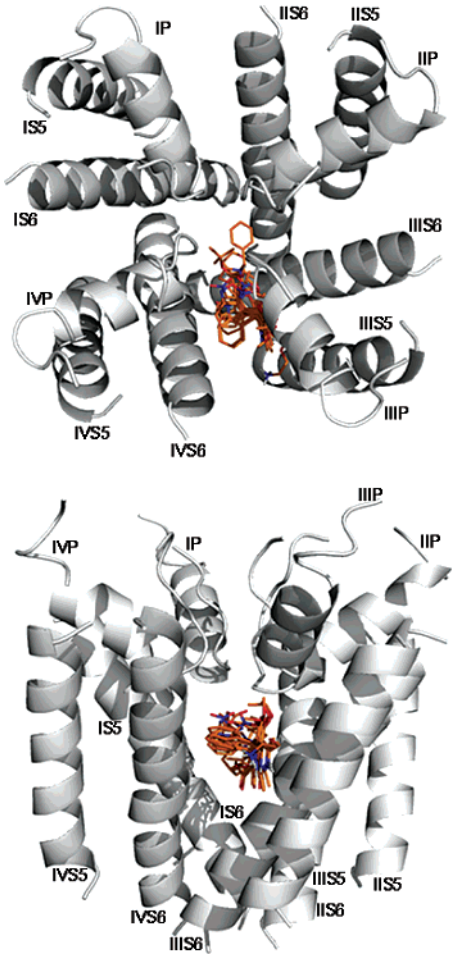

Figure 5. Top and side view of docked DHPs in Model A of LCC. Ligands are represented as orange sticks, while LCC is represented as gray ribbons.

unambiguously determined, hence, two different candidate models were built for both alignments of IIIS6. These models will be referred as follows: Model A in which Glu1161 is aligned with Trp87 of KcsA and Model B in which Val1160 of LCC is aligned with Trp87 of KcsA.

Less information is available for segments IS6 and IIS6, so it was suggested to align the hydrophobic Trp380 (IS6) and Leu728 (IIS6) with Trp87 of KcsA.[10] A Gly residue at the C-terminus of the LCC S5 segments is highly conserved, thus, they were all aligned so as to allow this residue to coincide with Gly43 of KcsA. Moreover, Thr1066 and Gln1070, which are important for the interaction with DHPs,[42] are placed in vicinity of the putative binding site of DHPs.

P-Loops Construction. The extracellular region between M1 and M2 segments of KcsA and MthK deepens into the pore, forming a narrow region of ~12 Å. This region is lined by the main chain carbonyl oxygens of the sequence TXGYG acting as a selectivity filter, allowing only the passage of K^+ ions.[12,14] On the other hand, the selectivity filter in LCC is made by the side chains of four highly conserved glutamates (EEEE locus). Consequently, while in KcsA, permeating cations interact with the backbone carbonyl groups of the residues in the selectivity-filter region and in LCC ions should interact with the side chains of selectivity-filter residues. As a result of the differences between the two P-loops, the use of KcsA P-loop to model the LCC one has long been questionable.[43] In 2005, Zhorov and co-worker proposed a model of Na^+ channel P-loop region, using MthK coordinates, in which the P-Loop region shares an almost identical folding of the correspondent portion in KcsA.[44] These studies clearly demonstrated that experimentally available data on the Na^+ channel selectivity-filter region could be explained without great modification of the X-ray template of the P-loop region in MthK. Most precisely, it was demonstrated that pharmacological and electrophysiological features of the Na^+ channel could be reproduced in the model through minor adjustments of the channel template in the selectivity-filter region without displacing the entire P-loops. This suggests that the P-loop region of voltage gated Na^+ channels of KcsA and of MthK have similar 3D structures. Moreover, the same considerations could be raised for the P-loop region of LCC. In fact, experimental evidence indicates that the substitution of selectivity filter residues Lys1422 and Ala1714 in the Na^+ channel (forming the DEKA locus) with Glu (DEEE) provides Ca^{2+}-selectivity to the channel.[45] In addition, this channel featured some peculiar pore behavior of native Ca^{2+} channels, such as permeation by Na^+ in the absence of Ca^{2+}.[46] Furthermore, the double LCC mutant, E1086K/E1387A (human L-type Cav1.2), (EEKA locus) led to a channel with pore characteristics analogous to those of Na^+.[47]

Consequently, we constructed a 3D model of LCC P-Loop using KcsA as a template. It is worth noting that it does not seem viable to model the entire extracellular portion between the S5 and the S6 helices. Actually, these large loops have different lengths among the four subunits, and the little experimental data are not sufficient to model the whole region. Anyway, several mutagenesis data suggest that the DHP binding site is located between the IIIS6 and the IVS6 helices and, ignoring the extracellular portion between P-loops and the S5 segment, is unlikely to affect results of our modeling. Consequently, we decided to model solely the LCC extracellular pore region.

To model the LCC P-loop, the alignment reported by Tikhonov and Zhorov[44] and Yamaguchi et al.[48] was used. This alignment places Phe1128, Ser1131, and Phe1133 (repeat III) to form part of the putative binding pocket of DHP in line with mutagenesis data, indicating the important role of such residues in the interaction with these ligands.[9,48] Glu residues of the selectivity filters are located at the same level, even though several authors suggested an asymmetrical alignment so to give explanation for the presence of accessory Ca^{2+} binding sites. On the other hand, pairwise replacement of the four glutamates excluded the hypothesis of two high affinity Ca^{2+} binding sites, therefore, it was concluded that the Glu residues had to be located at the same level, forming a single selectivity filter ring.[49]

Assembly of the P-Loop Region with the Transmembrane Bundle of LCC. After construction of the LCC pore region, this portion was adapted on the model of the transmembrane bundle of the Ca^{2+} channel. According to Lipkind studies,[10] the pore region of LCC has been sited higher with respect to KcsA P-Loop and closer to the extracellular side of the membrane.

In the absence of detailed information of the interactions between the P-loop and the transmembrane bundle, ZDOCK[29] has been used to adapt the P-loop on both Model A and Model B of the transmembrane bundle. The choice of this protein−protein docking software was supported by the outstanding results achieved through their employment in the CAPRI experiments, where it has been shown to be a fast and reliable predictor of protein−protein complexes.[50] A total of 30 models were obtained, and the top ranking structure placed the outer region in a reasonable position (Figure 4), in fact, the P-loop portion of each repeat was in both cases (Models A and B)

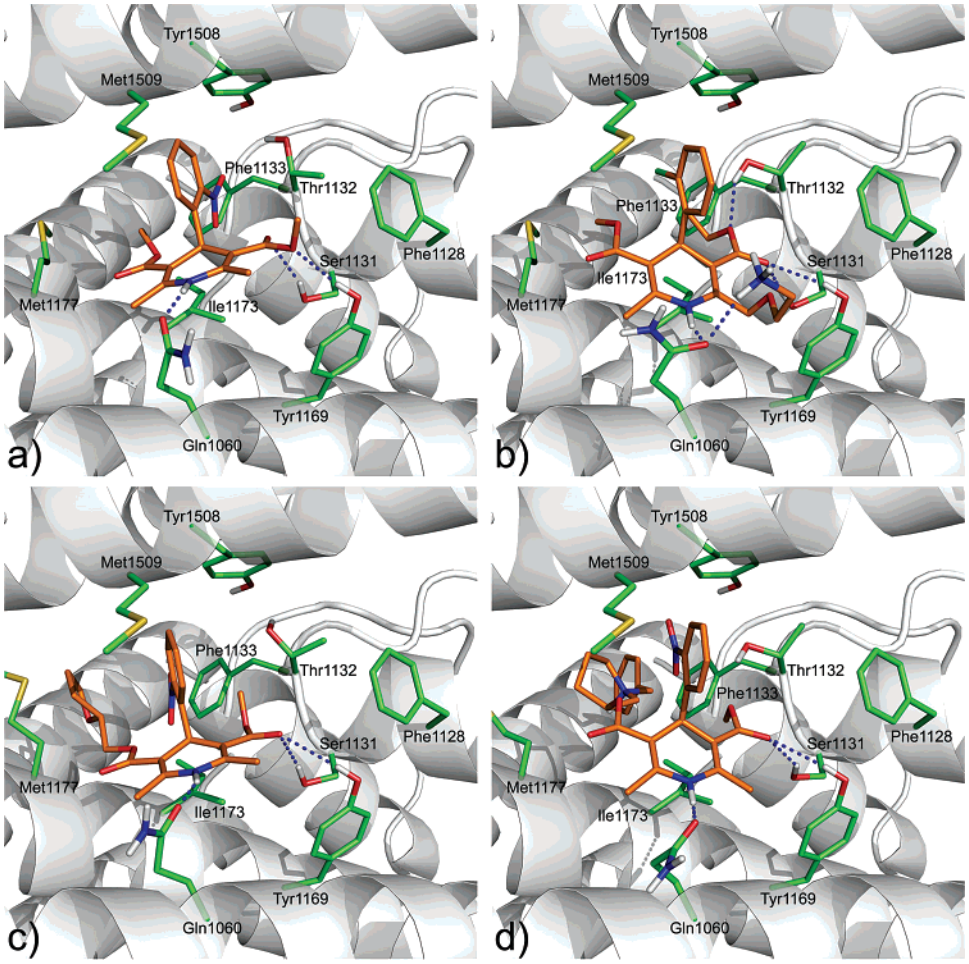

Figure 6. Docked structures of nifedipine (a), (*R*)-amlodipine (b), (*S*,*S*)-furnidipine (c), and (*S*,*S*)-benidipine in Model A of LCC. DHPs are displayed as white sticks, and key binding site residues are shown in green. Hydrogen bonds are represented with dashed blue lines.

adjusted in the crevice formed by the S5 segment of the same repeat and the S6 segment of the adjacent one. All other models generated by ZDOCK were discarded due to the implausible binding interactions between the two portions.

The generated models for candidates A and B were then analyzed to see if they were in accordance with experimental data. Mutagenesis experiments infer that the selectivity filter (EEEE locus) is in close proximity to the Tyr1508.[37] In fact, DHP binding is not affected by mutation of residues above Tyr1508, thus suggesting that this portion might be in close contact with the pore region.[37,38] Moreover, when mutating Tyr1508 to Ala, the reversal potential of the channel is altered by 15 mV and permeation of *N*-methyl-D-glucamine is increased, suggesting that this residue is near the selectivity filter.[37]

A comparison of the amino acid sequences of the P-loop region of different LCCs reveals that all DHP-sensitive channels have a Phe1113 adjacent to Glu1114 of the selectivity filter, while all DHP-insensitive channels have a Gly at this position.[9] From mutagenesis experiments, it could be speculated that Phe1113 might be involved in the allosteric coupling of Ca^{2+} and DHP binding due to its close proximity to Glu1114.[41] Interestingly, in both models (A and B), the Tyr1508 residue is located in the proximity of the EEEE locus and really close to Phe1113, engaging with it charge-transfer interactions. These considerations support the feasibility of the predicted adjustment of the P-loop on both transmembrane bundles.

DHP Docking. To shed light on the molecular basis of the interactions between LCC and its ligands, docking simulations of several DHPs on both Model A and Model B were carried out. As shown in Table 2, the 50 independent docking runs performed for each ligand usually converged to a small number of different clusters ("clusters" of results differing by less than 1.5 Å rmsd). Even if the predicted free energy of binding associated with each solution should be used as a criterion for the choice of the "best" posing, due to a certain inaccuracy of the scoring function, herein the preference for one solution has been also governed by its consistency with SARs and mutagenesis data. In the following section, a brief description of the calculated binding modes of the selected DHPs into both Model A and Model B is given.

DHP Docking on Model A of LCC. Docking of nifedipine, nitrendipine, (*S*)-isradipine, (*R*)-amlodipine, lacidipine, (*S*)-furnidipine, and (*S*,*S*)-benidipine into Model A gave comparable binding solutions, with the dihydropyridine ring fitting in the cleft formed by IIIS6, IIIS5, and IVS6 segments. Moreover, in each solution, the plane of the DHP ring is parallel to the pore axis, the ligand NH group faces the IIIS5 segment, the starboard side of the heterocyclic ring points upward, and the plane of the 4-aryl substituent is perpendicular to the pore axis (Figure 5).

This orientation allows the molecules to establish several favorable contacts which are rather recurrent in the calculated posing of the inspected DHPs.

In all inspected ligands, the N1 hydrogen atom of the heterocyclic ring H-bonds with the carbonyl oxygen of Gln1060 side-chain in IIIS5 (Figure 6). This is in accordance with both SARs and mutagenesis data. In fact, while SARs studies indicate that the N1 hydrogen atom has a key role in the binding of

DHPs to LCC[17] mutational analysis clearly demonstrated that Gln1070 contributes to the binding of DHPs.[37] Interestingly, it was also reported that mutation of Gln1070 to Asp did not affect the binding of DHPs indicating the participation of the glutamine side chain as H-bond acceptor in consonance with the proposed binding mode.

As depicted in Figure 6, both the carbonyl and ester oxygens on the starboard side of the dihydropyridine ring form two H-bonds with the Ser1131 and Tyr1169 side chains. This is in accordance with SAR data indicating the involvement of this group in H-bond interactions with the channel.[6,17] SAR data indicate that only small-sized ester groups are tolerated on the starboard side of the DHP ring.[17] This data might be rationalized by the fact that the above cited group adapts itself in a rather small cleft formed by Tyr1169, Phe1128, Thr1129, Ser1131, and Thr1132. Nevertheless, the location of the starboard side ester in this small cleft permits the establishing of favorable hydrophobic interactions between the methyl or the ethyl group on the DHP ester and the Phe1128 side chain, which has been reported to participate to the binding of DHPs.[49] The involvement of Tyr1169 in a H-bond with the carbonyl oxygen of the starboard side esters of (*R*)-amlodipine, (*S*,*S*)-benidipine, and (*S*,*S*)-furnidipine and with the ester oxygen of the same group in nifedipine, (*S*)-isradipine, lacidipine, and (*S*)-nitrendipine (see Figure 6) is also in agreement with mutagenesis data. In fact, when mutating Tyr1169 to Ala, (*S*)-isradipine resulted to be 25-fold less active on the resulting mutant.[41] Moreover, when Tyr1169 was mutated to Phe, (*S*)-isradipine demonstrated to be 12.4-fold less active on the resulting mutant if compared with the wild-type channel.[41] This demonstrates the involvement of the Tyr1169 hydroxyl group in a H-bond with the ligand in agreement with the proposed binding pose. The involvement of Ser1131 in the binding of DHPs was demonstrated by Yamaguchi et al. who reported that, when mutating Ser1131 to Ala, the IC_{50} value of (*S*)-nitrendipine was 39.4 times higher than that of rbCII (rat brain Ca^{2+} channel α1C subunit type II).[48]

The 4-aryl substituent of the docked DHPs is in close contact with Tyr1508, engaging with this residue a T-shaped charge-transfer interaction. Also, in this case, the involvement of Tyr1508 in the binding of LCC DHP antagonists was experimentally proven by mutagenesis studies. In fact, replacement of this residue to Ala has large effects on DHP activity, with the K_D for DHP binding in Tyr1508Ala mutant increased by 6.1-fold.[38] Extensive SAR studies have unambiguously demonstrated that electron-withdrawing substituents in the 4-phenyl ring enhance activity in the *ortho* and *meta* positions, while any substituent in the *para* position is detrimental.[6,17] This data can be rationalized by the proposed posing. In fact, a substituent in the *para* position to the phenyl ring would give unfavorable steric clashes with the backbone atoms of Tyr1508 and Met1509, while substituents in both *ortho* and *meta* positions have enough space in the binding pocket.

The ester group on the port side of the DHP ring adopts a *cis* conformation to the double bond of the heterocyclic ring. The *trans* conformation does not appear to be feasible due to the unfavorable steric clashes that the large port side esters would give with the IIIS6 segment. Indeed, synthesis of DHP derivatives with an immobilized ester group demonstrated the preference for a *cis* conformation of the port side ester. It is worth noting that the large lipophilic substituents on the port side ester establish favorable hydrophobic interactions with Met1177 and Met1178, which have been shown to participate to the binding of DHPs.[41] Alternatively, the same substituent points toward the center of the pore, establishing $\pi-\pi$ charge-transfer interactions with Phe1133, as in the case of (*S*,*S*)-benidipine. Noticeably, lacidipine has a small port-side ester, although in this case, the large lipophilic substituent present in the *ortho* position on the 4-phenyl ring occupies the same region of the above cited groups.

The entire DHP ring adapts itself on the Ile1173 side-chain, establishing with it favorable hydrophobic interactions. This data also agrees with mutagenesis studies indicating that mutation of Ile1173 to Ala results in a loss of potency on DHP of 17-fold.

In regard to positions 2 and 6 of the DHP ring, the majority of the analyzed drugs are characterized by the presence of methyl substituents. The only exception is found in (*R*)-amlodipine (Figure 6b) in which the flexible aminoethyloxymethyl group, through its protonated amine atom, H-bonds with the Gln1060 side chain carbonyl oxygen.

DHP Docking on Model B of LCC. The general binding orientation of the docked DHPs into Model B resembles the one found using Model A. In fact, as calculated by AutoDock, the DHP ring locates itself in the fissure between segments IIIS6, IIIS5, and IVS6, with the heterocyclic ring adapted in the same orientation found in Model A. The great majority of the detected interaction in Model A were also found in Model B. In fact, (i) the N1 hydrogen atom of the DHP ring H-bonds with the carbonyl oxygen of Gln1060 side chain, (ii) the carbonyl oxygen of the starboard side ester H-bonds with the hydroxyl group of the Ser1131 side chain, (iii) the ester on the port side of the DHP ring is favorably positioned in a *cis* orientation to the ring double bond so to allow the large ester portion to point toward the center of the channel pore (Figure 7). This orientation permits the establishing of favorable hydrophobic interactions with Ile1173 and Met1177, which were reported to influence the DHP binding.[41]

Indeed, the different alignment of the IIIS6 portion implicates the presence of different interactions with this segment. The most striking difference in the DHP binding to Model B resides in the absence of any interaction between the ligand and the Tyr1169, which, as already mentioned, plays a crucial role in the recognition mechanism of DHP to LCC.[41] Additionally, in Model B, apart from Ile1173, the essential residues Met1177, Met1178, and Met1175 are placed far away from the docked DHPs.

From this point of view, our calculations strongly indicate that the sequence alignment between IIIS6 of LCC and M2 of KcsA in Model B is unable to produce all the essential interactions with the DHP ring. In this respect, the sequence alignment of IIIS6 in Model A appears to be more in accordance with experimental findings such as SARs and mutagenesis data.

From Antagonist to Agonist DHPs. In our theoretical study, we were also tempted to rationalize a peculiar pharmacological behavior of some DHPs. In fact, it is well-known that some DHPs exhibit an interesting stereoselective duality of action, with one enantiomer behaving as an agonist and the other one having antagonist properties. Indeed, these LCC activators do not have any therapeutic role; nevertheless, they represent one of the paradoxes of medicinal chemistry. For these reasons, both the antagonist (*R*)-enantiomer and the agonist (*S*)-enantiomer of Bay K 8644[51] were also docked.

As expected, the predicted posing of (*R*)-Bay K 8644 into Model A of LCC strongly resembles the above-described ones establishing the same polar and hydrophobic interactions found for the previously mentioned antagonists (Figure 8a). It is worth noting that the vicinity of the ligand port side ester with the

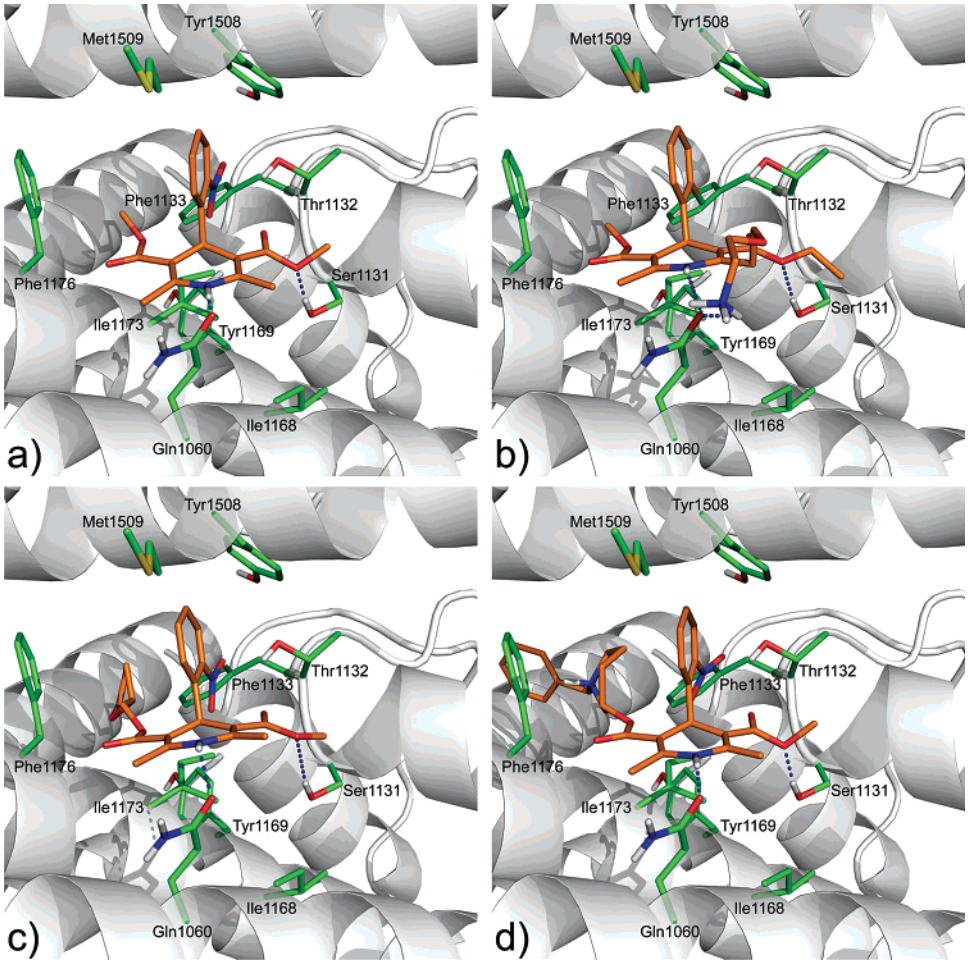

Figure 7. Docked structures of nifedipine (a), (*R*)-amlodipine (b), (*S*,*S*)-furnidipine (c), and (*S*,*S*)-benidipine in Model B of LCC. DHPs are displayed as white sticks, and key binding site residues are shown in green. Hydrogen bonds are represented with dashed blue lines.

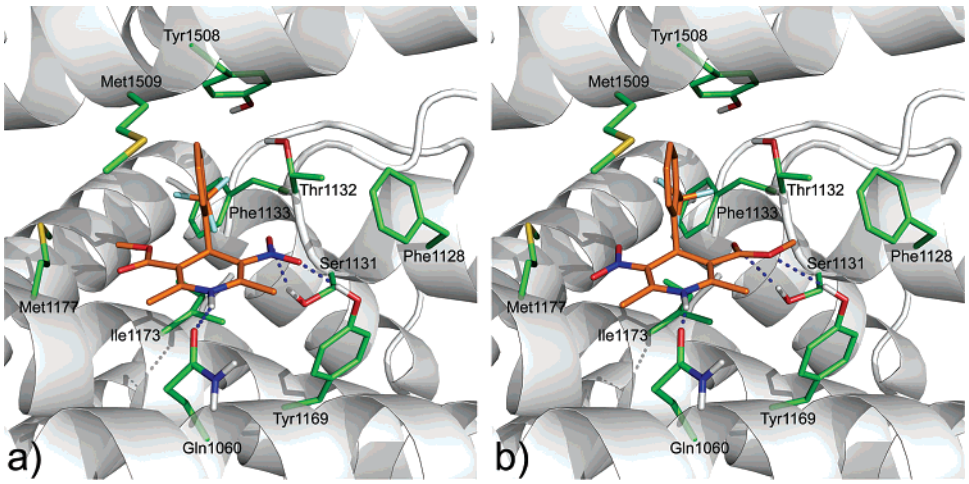

Figure 8. Docked structures of (*R*)-Bay K 8644 (a) and (*S*)-Bay K 8644 (b) in Model A of LCC. DHPs are displayed as white sticks, and key binding site residues are shown in green. Hydrogen bonds are represented with dashed blue lines.

hydrophobic residues at the crevice between the IIIS6 and the IVS6 segments could impede the conformational rearrangements of these segments, thus stabilizing the inactivated state of the channel.[9] In fact, it is well-known that voltage-gated channels seem to open by movement of the inner parts of the S6 α-helices.[52]

Also for the (*S*)-enantiomer of Bay K 8644, the calculated posing was similar with what was already found for the (*R*)-enantiomer, and this is in accordance with experimental data, suggesting that both DHP agonists and DHP antagonists should share the same binding site.[9] Obviously, the different absolute configuration of the chiral center in position 4 allows different interactions with LCC. In fact, in this case, the nitro group on the port side faces the bottom of the channel pore, while the starboard side points outward, H-bonding with Ser1131 and Tyr1169 (Figure 8b). The main differences in the calculated binding mode of (*S*)-Bay K 8644 with respect to the (*R*)-enantiomer mainly reside in the absence of any interaction with the hydrophobic residues present at the intersection between the IIIS6 and the IVS6 segments, where the main structural

rearrangement occurs during the channel opening. Therefore, the lack of such an interaction could explain the reasons for the absence of any antagonist activity of this enantiomer. Moreover, the latter ligand exposes this hydrophilic nitro group to a hydrophobic surface at the junction of the S6 segments of repeat III and IV in the closed state, making such an interaction energetically unfavorable. Therefore, it could be hypothesized that the agonist could destabilize the closed state of LCC and could stabilize the opened one. Further studies should be undertaken to elucidate the conformation of the channel in the open state and then use it to dock the agonist ligands eventually confirming such a hypothesis.

Conclusions

In this contribution we report results of a computational study on the human cardiac L-Type Ca^{2+} channel. A 3D model of this channel was built using the crystallographic structure of KcsA as a template.[13] Extensive mutagenesis data on LCC allowed to perform a pairwise alignment between the sequences of the two proteins, leading to two different arrangements that were used to construct two candidate models of LCC (Models A and B). After construction of the transmembrane bundle and P-loop region alone, the latter was adapted on the intracellular portion through rigid-body protein−protein docking calculations.

Automated docking simulations were then conducted using both Model A and Model B on nine different DHP antagonists featuring molecular diversity. These calculations allowed to detect the presence of a similar posing in both theoretical models where: the plane of the DHP ring is parallel to the pore axis, the ligand NH group faces the IIIS5 segment, the starboard side of the heterocyclic ring points upward and the plane of the 4-aryl substituent is perpendicular to the pore axis (Figure 5). Despite the comparable binding orientation of DHP antagonists in both candidates, dissimilar interaction patterns were detected between ligands and LCC, with the most prominent difference residing in the lack of specific interactions with the IIIS6 segment in Model B. In particular, in the latter model, the ligand is unable to interact with the Tyr1169 residue, which was reported to have a key role in the interaction with DHP antagonists.[41] In this respect, the coherence between docking results obtained with structure A and SARs and mutagenesis data would drive our preference toward this candidate rather than the B structure. Such models provided plausible hypotheses for ligand−channel interactions, satisfactorily explaining the large body of SAR data available in literature and revealing the key residues that interact with ligands. The described posing of the DHP antagonist into the LCC inner pore might also help in suggesting a possible mechanism of action. In fact, LCC is believed to open through a movement of the C-terminal part of S6 segments of each repeat, resulting in a widening of this region that allows the passage of Ca^{2+} ions.[52] In the predicted binding pose of the selected DHPs the port side ester establishes favorable hydrophobic interactions with the lipophilic C-terminal residues of IIIS6 and IVS6 segments. Therefore, it might be speculated that such an interaction might stabilize the inactivated state of LCC by preventing the relocation of IIIS6 and IVS6 segments required for the opening of the channel.

It is worth noting that the validity of this theoretical model relies on some assumptions and remains speculative. However, the coherence of many observations on the 3D models might not be fortuitous.

Acknowledgment. This work was supported by a grant from Ministero dell'Università e della Ricerca Scientifica.

References

(1) (a) Heilbrunn, L. V. *An Outline of General Physiology*, 1st, 2nd, and 3rd editions; Saunders Co.: Philadelphia, PA, 1952; pp 1937−1943. (b) Carafoli, E. Calcium signaling: A tale for all seasons. *Proc. Natl. Acad. Sci. U.S.A.* **2002**, *99*, 1115−1122. (c) Berridge, M. J.; Lipp, P.; Bootman, M. D. The versatility and universality of calcium signaling. *Nat. Rev. Mol. Biol.* **2000**, *1*, 11−21. (d) Verkhratsky, A.; Landfield, P. W.; Thibault, O. Ca^{2+} and neuronal pathology. *Eur. J. Pharmacol.* **2002**, *447*, 115−296.

(2) (a) Birnbaumer, L.; Campbell, K. P.; Catterall, W. A.; Harpold, M. M.; Hofmann, F.; Horne, W. A.; Mori, Y.; Schwartz, A.; Snutch, T. P.; Tanabe, T.; Tsien, R. W. The naming of voltage-gated calcium channels. *Neuron* **1994**, *13*, 505−506. (b) Catterall, W. A. Structure and function of voltage-gated ion channels. *Annu. Rev. Biochem.* **1995**, *64*, 493−531. (c) Hofmann, F.; Biel, M.; Flockerzi, V. Molecular basis for Ca^{2+} channel diversity. *Annu. Rev. Neurosci.* **1994**, *17*, 399−418.

(3) (a) Catterall W. A.; Striessnig, J.; Snutch, T. P.; Perez-Reyes, E. International Union of Pharmacology. XL. Compendium of voltage-gated ion channels. Calcium channels. *Pharmacol. Rev.* **2003**, *55*, 579−581. (b) Catterall, W. A.; Perez-Reyes, E.; Terrance, P.; Striessnig, J. International Union of Pharmacology. XLVIII. Nomenclature and structure-function relationships of voltage-gated calcium channels. *Pharmacol. Rev.* **2005**, *57*, 411−425.

(4) Hille, B. *Ionic Channels of Excitable Membranes*, 3rd edition; Sinauer: Sunderland, MA, 2001.

(5) Hille, B. *Ionic Channels of Excitable Membranes*, 2nd edition; Sinauer: Sunderland, MA, 1992.

(6) (a) Triggle, D. J.; Rampe, D. 1,4-Dihydropyridine activators and antagonists: Structural and functional distinctions. *Trends Pharmacol. Sci.* **1989**, *10*, 507−511. (b) Triggle, D. J. Calcium, calcium channels, and calcium channel antagonists. *Can. J. Physiol. Pharmacol.* **1990**, *68*, 1474−1481. (c) Triggle, D. J. Calcium-channel drugs: Structure-function relationships and selectivity of action. *J. Cardiovasc. Pharmacol.* **1991**, *18*, S1−S6. (d) Triggle, D. J. Sites, mechanisms of action, and differentiation of calcium channel antagonists. *Am. J. Hypertens.* **1991**, *4*, 422S-429S. (e) Triggle, D. J. Molecular pharmacology of voltage-gated calcium channels. *Ann. N.Y. Acad. Sci.* **1994**, *15*, 267−281. (f) Triggle, D. J. Ion channels as pharmacologic receptors: The chirality of drug interactions. *Chirality* **1996**, *8*, 35−38. (g) Triggle, DJ. L-type calcium channels. *Curr. Pharm. Des.* **2006**, *12*, 443−457.

(7) Catterall, W. A.; Striessnig, J. Receptor sites for Ca^{2+} channel antagonists. *Trends Pharmacol. Sci.* **1992**, *13*, 256−262.

(8) (a) Glossmann, H.; Ferry, D. R.; Goll, A.; Rombusch, M. Molecular pharmacology of the calcium channel: Evidence for subtypes, multiple drug-receptor sites, channel subunits, and the development of a radioiodinated 1,4-dihydropyridine calcium channel label, [^{125}I]-iodipine. *J. Cardiovasc. Pharmacol.* **1984**, *6*, 508−621. (b) Hockerman, G. H.; Peterson, B. Z.; Johnson, B. D.; Catterall, W. A. Molecular determinants of drug binding and action of L-type calcium channels. *Annu. Rev. Pharmacol. Toxicol.* **1997**, *37*, 361−396.

(9) Peterson, B. Z.; Catterall, W. A. Calcium binding in the pore of L-type calcium channels modulates high affinity dihydropyridine binding. *J. Biol. Chem.* **1995**, *270*, 18201−18204.

(10) Lipkind, G. M.; Fozzard, H. A. Molecular modeling of the interaction of dihydropyridines and phenylalkylamines with the inner pore of the L-type Ca^{2+} channel. *Mol. Pharmacol.* **2003**, *63*, 499−511.

(11) Zhorov, B. S.; Folkman, E. V.; Ananthanarayanan, V. S. Homology model of dihydropyridine receptor: implications for L-type Ca^{2+} channel modulation by agonists and antagonists. *Arch. Biochem. Biophys.* **2001**, *393*, 22−41.

(12) Doyle, D. A.; Cabral, J. M.; Pfuetzner, R. A.; Kuo, A.; Gulbis, J. M.; Cohen, S. L.; Chait, B. T.; MacKinnon, R. The structure of the potassium channel: Molecular basis of K^+ conduction and selectivity. *Science* **1998**, *280*, 69−74.

(13) (a) Zhorov, B. S.; Tikhonov, D. B. Potassium, sodium, calcium, and glutamate-gated channels: Pore architecture and ligand action. *J. Neurochem.* **2004**, *88*, 782−799. (b) Lipkind, G. M.; Fozzard, H. A. KcsA crystal structure as framework for a molecular model of the Na^+ channel pore. *Biochemistry* **2000**, *39*, 8161−8170. (c) Tikhonov, D. B.; Bruhova, I.; Zhorov, B. S. Atomic determinants of state-dependent block of sodium channels by charged local anesthetics and benzocaine. *FEBS Lett.* **2006**, *13*, 6027−6032. (d) Rossokhin, A.; Teodorescu, G.; Grissmer, S.; Zhorov, B. S. Interaction of d-tubocurarine with potassium channels: Molecular modeling and ligand binding. *Mol. Pharm.* **2006**, *69*, 1356−1365. (e) Wang, S. Y.; Mitchell, J.; Tikhonov, D. B.; Zhorov, B. S.; Wang, G. K. How batrachotoxin modifies the sodium channel permeation pathway: Computer modeling and site-directed mutagenesis. *Mol. Pharm.* **2006**, *69*, 788−795. (f) Scheib, H.; McLay, I.; Guex, N.; Clare, J. J.; Blaney, F. E.; Dale, T. J.; Tate, S. N.; Robertson, G. M. Modeling the pore

structure of voltage-gated sodium channels in closed, open, and fast-inactivated conformation reveals details of site 1 toxin and local anesthetic binding. *J. Mol. Model.* **2006**, *12*, 813−822. (g) Giorgetti, A.; Carloni, P.; Mistrik, P.; Torre, V. A homology model of the pore region of HCN channels. *Biophys. J.* **2005**, *89*, 932−944. (h) Shealy, R. T.; Murphy, A. D.; Ramarathnam, R.; Jakobsson, E.; Subramaniam, S. Sequence-function analysis of the K^+-selective family of ion channels using a comprehensive alignment and the KcsA channel structure. *Biophys. J.* **2003**, *84*, 2929−2942.

(14) Jiang, Y.; Lee, A.; Chen, J.; Cadene, M.; Chait, B. T.; MacKinnon, R. Crystal structure and mechanism of a calcium-gated potassium channel. *Nature* **2002**, *417*, 515−522.

(15) Morris, G. M.; Goodsell, D. S.; Halliday, R. S.; Huey, R.; Hart, W. E.; Belew, R. K.; Olson, A. J. Automated docking using a Lamarckian genetic algorithm and an empirical binding free energy function. *J. Comput. Chem.* **1998**, *19*, 1639−1662 (The Scripps Research Institute, La Jolla, CA 92037−1000).

(16) Goodsell, D. S.; Morris, G. M.; Olson, A. J. Automated docking of flexible ligands: Applications of AutoDock. *J. Mol. Recognit.* **1996**, *9*, 1−5.

(17) Goldmann, S.; Stoltefuss, J. 1,4-Dihydropyridines: Effects of chirality and conformation on the calcium antagonist and calcium agonist activities. *Angew. Chem., Int. Ed. Engl.* **1991**, *30*, 1559−1578.

(18) (a) Bossert, F.; Vater, W. U.S. Patent 3,485,847, Dec 23, 1969. (b) Vater, W.; Kroneberg, G.; Hoffmeister, F.; Saller, H.; Meng, K.; Oberdorf, A.; Puls, W.; Schlossmann, K.; Stoepel, K. Pharmacology of 4-(2′-nitrophenyl)-2,6-dimethyl-1,4-dihydropyridine-3,5-dicarboxylic acid dimethyl ester (Nifedipine, BAY a 1040). *Arzneim.-Forsch.* **1972**, *22*, 1−14.

(19) (a) Stoepel, A.; Heise, S.; Kazda, S. Pharmacological studies of the antihypertensive effect of nitrendipine. *Arzneim.-Forsch.* **1981**, *32*, 2056−2064. (b) Meyer, H.; Bossert, F.; Wehinger, E.; Stoepel, K.; Vater, W. Synthesis and comparative pharmacological studies of 1,4-dihydro-2,6-dimethyl-4-(3-nitrophenyl)pyridine-3,5-dicarboxylates with nonidentical ester functions. *Arzneim.-Forsch.* **1981**, *31*, 407−409. (c) Mikus, G.; Mast, V.; Ratge, D.; Wisser, H.; Eichelbaum, M. Stereoselectivity in cardiovascular and biochemical action of calcium antagonists: studies with the enantiomers of the dihydropyridine nitrendipine. *Clin. Pharmacol. Ther.* **1995**, *57*, 52−61.

(20) Bristolo, J. A. *Annu. Rep. Med. Chem.* **1992**, *27*, 330.

(21) (a) Fitton, A.; Benfield, P. Isradipine. A review of its pharmacodynamic and pharmacokinetic properties, and therapeutic use in cardiovascular disease. *Drugs* **1990**, *40*, 31−74. (b) Hof, R. P.; Hof. A.; Ruegg, U. T.; Cook, N. S.; Vogel, A. Stereoselectivity at the calcium channel: Different profiles of hemodynamic activity of the enantiomers of the dihydropyridine derivative PN 200−110. *J. Cardiovasc. Pharmacol.* **1986**, *8*, 221−226.

(22) Arrowsmith, J. E.; Campbell, S. F.; Cross, P. E.; Stubbs, J. K.; Burges, R. A.; Gardiner, D. G.; Blackburn, K. J. Long-acting dihydropyridine calcium antagonists. 1. 2-Alkoxymethyl derivatives incorporating basic substituents. *J. Med. Chem.* **1986**, *29*, 1696−1702.

(23) (a) Alajarin, R.; Vaquero, J. J.; Alvarez-Builla, J.; Pastor, M.; Sunkel, C.; de Casa-Juana, M. F.; Priego, J.; Statkow, P. R.; Sanz-Aparicio, J. Synthesis and chromatographic separation of the stereoisomers of furnidipine. *Tetrahedron: Asymmetry* **1993**, *4*, 617−620. (b) Alajarin, R.; Alvarez-Builla, J.; Vaquero, J. J.; Sunkel, C.; de Casa-Juana, M. F.; Statkow, P. R.; Sanz-Aparicio, J.; Fonseka, I. Synthesis, structure, and pharmacological evaluation of the stereoisomers of furnidipine. *J. Med. Chem.* **1995**, *38*, 2830−2841.

(24) Ishii, A.; Nishida, K.; Oka, T.; Nakamizo, N. Receptor binding properties of the new calcium antagonist benidipine hydrochloride. *Arzneim.-Forsch.* **1988**, *38*, 1677−1680.

(25) *SYBYL*, version 6.9.1.; Molecular Modelling System, Tripos, Inc.: St. Louis, MO, 2003.

(26) (a) Accelrys, Inc., San Diego, CA. (b) *Discover3*, 2.98 edition; Accelrys, Inc.: San Diego, CA.

(27) (a) *DISCOVER*, version 95.0.; BIOSYM Technologies: 10065 Barnes Canyon Rd, San Diego, CA 92121. (b) Hagler, A. F.; Lifson, S.; Dauber, P. Consistent force field studies of intermolecular forces in hydrogen-bonded crystals. *J. Am. Chem. Soc.* **1979**, *101*, 5122−5130.

(28) Bairoch, A.; Apweiler, R. The SWISS-PROT protein sequence database and its supplement TrEMBL in 2000. *Nucleic Acids Res.* **2000**, *28*, 45−48.

(29) Chen, R.; Li, L.; Weng, Z. ZDOCK: An initial-stage protein docking algorithm. *Proteins* **2003**, *52*, 80−87.

(30) Katchalski-Katzir, E.; Shariv, I.; Eisenstein, M.; Friesem, A.; Aflalo, C.; Vakser, I. A. Molecular surface recognition-determination of geometric fit between proteins and their ligands by correlation techniques. *Proc. Natl. Acad. Sci. U.S.A.* **1992**, *89*, 2195−2199.

(31) Zhang, C.; Vasmatzis, G.; Cornette, J. L.; DeLisi, C. Determination of atomic desolvation energies from the structures of crystallized proteins. *J. Mol. Biol.* **1997**, *267*, 707−726.

(32) (a) Comeau, S. R.; Gatchell, D. W.; Vajda, S.; Camacho, C. J. ClusPro: An automated docking and discrimination method for the prediction of protein complexes. *Bioinformatics* **2004**, *20*, 45−50. (b) Comeau, R.; Gatchell, D. W.; Vajda, S.; Camacho, C. J. ClusPro: A fully automated algorithm for protein−protein docking. *Nucleic Acids Res.* **2004**, *32*, W96−99.

(33) Laskowski, R. A.; MacArthur, M. W.; Moss, D. S.; Thornton, J. M. PROCHECK: A program to check the stereochemical quality of protein structures. *J. Appl. Crystallogr.* **1993**, *26*, 283−291.

(34) Allen, F. H.; Bellard, S.; Brice, M. D.; Cartwright, B. A.; Doubleday, A.; Higgs, H.; Hummelink, T.; Hummelink-Peters, B. G.; Kennard, O.; Motherwell, W. D. S. The Cambridge crystallographic data center: Computer-based search, retrieval, analysis and display of information. *Acta Crystallogr.* **1979**, *B35*, 2331−2339.

(35) Head, J.; Zerner, M. C. A Broyden-Fletcher-Goldfarb-Shannon optimization procedure for molecular geometries. *Chem. Phys. Lett.* **1985**, *122*, 264−274.

(36) Gasteiger, J.; Marsili, M. Iterative partial equilization of orbital electronegativitys. A rapid access to atomic charges. *Tetrahedron* **1980**, *36*, 3219−3228.

(37) Hockerman, G. H.; Johnson, B. D.; Scheuer, T.; Catterall, W. A. Molecular determinants of high-affinity phenylalkylamine block of L-type calcium channels. *J. Biol. Chem.* **1995**, *270*, 22119−22122.

(38) (a) Mitterdorfer, J.; Wang, Z.; Sinnegger, M. J.; Hering, S.; Striessnig, J. Grabner, M.; Glossmann, H. Two amino acid residues in the IIIS5 segment of L-type calcium channels differentially contribute to 1,4-dihydropyridine sensitivity. *J. Biol. Chem.* **1996**, *271*, 30330−30335. (b) Mitterdorfer, J.; Wang, Z.; Sinnegger, M. J.; Hering, S.; Striessnig, J.; Grabner, M.; Glossmann, H. Two amino acid residues in the IIIS5 segment of L-type calcium channels differentially contribute to 1,4-dihydropyridine sensitivity. *J. Biol. Chem.* **1996**, *271*, 30330−30335.

(39) Grabner, M.; Wang, Z.; Hering, S.; Striessnig, J.; Glossmann, H. Transfer of 1,4-dihydropyridine sensitivity from L-type to class A(B1) calcium channels. *Neuron* **1996**, *16*, 207−218.

(40) Schuster. A.; Lacinova, L.; Klugbauer, N.; Ito, H.; Birnbaumer, L.; Hofmann, F. The IVS6 segment of the L-type calcium channel is critical for the action of dihydropyridines and phenylalkylamines. *EMBO J.* **1996**, *15*, 2365−2370.

(41) Peterson, B. Z.; Johnson, B. D.; Hockerman, G. H.; Acheson, M.; Scheuer, T.; Catterall, W. A. Analysis of the dihydropyridine receptor site of L-type calcium channels by alanine-scanning mutagenesis. *J. Biol. Chem.* **1997**, *272*, 18752−18758.

(42) He, M.; Bodi, I.; Mikala, G.; Schwartz, A. Motif IIIS5 of L-type calcium channels involved in the dihydropyridine binding site. *J. Biol. Chem.* **1997**, *271*, 2629−2633.

(43) Lipkind, G. M.; Fozzard, H. A. Modeling of the outer vestibule and selectivity filter of the L-type Ca^{2+} Channel. *Biochemistry* **2001**, *40*, 6786−6794.

(44) Tikhonov, D. B.; Zhorov, B. S. Modeling P-loops domain of sodium channel: Homology with potassium channels and interaction with ligands. *Biophys. J.* **2005**, *88*, 184−197.

(45) Heinemann, S. M.; Terlau, H.; Stuhmer, W.; Imoto, W.; Numa, S. Calcium channel characteristics conferred on the sodium channel by single mutations. *Nature* **1992**, *356*, 441−443.

(46) Hess, P.; Tsien, R. W. Mechanism of ion permeation through calcium channels. *Nature* **1984**, *309*, 453−456.

(47) Tang, S.; Mikala, G.; Bahinski, A.; Yatani, A.; Varadi, G.; Schwartz, A. Molecular localization of ion selectivity sites within the pore of a human L-type cardiac calcium channel. *J. Biol. Chem.* **1993**, *268*, 13026−13029.

(48) Yamaguchi, S.; Zhorov, B. S.; Yoshioka, K.; Nagao, T.; Ichijo, H.; Adachi-Akahane, S. Key roles of Phe1112 and Ser1115 in the pore-forming IIIS5−S6. linker of L-type Ca^{2+} channel alpha-1C subunit (Cav1.2) in binding of dihydropyridines and action of Ca^{2+} channel agonists. *Mol. Pharmacol.* **2003**, *64*, 235−248.

(49) Ellinor, P. T.; Yang, J.; Sather, W. A.; Zhang, J. F.; Tsien, R. W. Ca^{2+} channel selectivity at a single locus for high-affinity Ca^{2+} interactions. *Neuron* **1995**, *15*, 1121−1132.

(50) Wiehe, K.; Pierce, B.; Mintseris, J.; Tong, W. W.; Anderson, R.; Chen, R.; Weng, Z. ZDOCK and RDOCK performance in CAPRI rounds 3, 4, and 5. *Proteins* **2005**, *60*, 207−213.

(51) Schramm, M.; Thomas, G.; Towart, R.; Franckowiak, G. Activation of calcium channels by novel 1,4-dihydropyridines. A new mechanism for positive inotropics or smooth muscle stimulants. *Arzneim.-Forsch.* **1983**, *33*, 1268−72.

(52) Liu, Y.; Holmgren, M.; Jurman, M. E.; Yellen, G. Gated access to the pore of a voltage-dependent K^+ channel. *Neuron* **1997**, *19*, 175−184.

JM061245A